Journal of MATERIALS RESEARCH

Article
DOI: 10.1557/jmr.2019.258

Nitrogen-doped zinc/cobalt mixed oxide micro-/nanospheres for high-rate lithium-ion battery anode

Xiaotao Deng[1], Sirui Li[2], Jiaqi Wang[2], Ding Nan[2,a)], Junhui Dong[2], Jun Liu[2,b)]

[1]*Pipeline Design Department, Zhuhai Branch of China Petroleum Pipeline Engineering Co., Ltd., Zhuhai 519015, People's Republic of China*
[2]*School of Materials Science and Engineering, Inner Mongolia University of Technology, Hohhot 010051, China; and Inner Mongolia Key Laboratory of Graphite and Graphene for Energy Storage and Coating, Hohhot 010051, China*
[a)]Address all correspondence to these authors. e-mail: nan1980732@163.com
[b)]e-mail: clxylj@163.com

Received: 14 May 2019; accepted: 9 August 2019

Metal oxides are promising candidates as the anodes of next-generation lithium ion batteries. However, the low electronic conductivities hinder their practical applications. Herein, through a facile calcination process using ammonium bicarbonate (NH_4HCO_3) as the N source, the nitrogen heteroelement was introduced into the ZnO/CoO micro-/nanospheres, which greatly improves the conductivity of the composites. As the lithium-ion battery anode, the N-doped ZnO/CoO micro-/nanosphere demonstrates much enhanced electrochemical performance. It displays a high initial capacity of 911.8 mA h/g at a current density of 0.2 A/g and long-term cycling stability, with a reversible capacity of 977.8 mA h/g remained after 500 cycles at a current density of 1 A/g. Furthermore, the N-doped ZnO/CoO composite presents an outstanding rate performance, with 605 mA h/g remained even at 5 A/g. The excellent electrochemical properties make N-doped ZnO/CoO micro-/nanospheres a promising candidate as high-performance anodes for next-generation rechargeable LIBs.

Introduction

Over the past decades, lithium-ion batteries (LIBs) have been regarded as the most significant energy storage devices for portable electronics and hybrid electric vehicles because of their advantages of high working voltage, fast charging/discharging rate, and large energy density [1, 2, 3]. Yet, the low theoretical capacity (372 mA h/g) of commercial graphite electrodes as well as the potential safety issues during cell operation limit their large-scale energy storage applications. Besides, the lithiation/delithiation reactions occurring on electrodes are typically accompanied by sluggish reaction kinetics, also endowing the LIBs with unsatisfactory rate capability. With the ever increasing demand for higher specific energy [4, 5], it is highly desirable to explore novel electrode materials with higher energy storage capacity [6]. Transition metal oxides are one type of promising candidates for next-generation LIB anode materials, and they possess many promising advantages as anodes of LIBs. Firstly, the theoretical capacities of metal oxides are higher than that of graphite; some are even approaching 1000 mA h/g, which is about 2–3 times higher than that of graphite. Secondly, the densities of metal oxides are also higher than that of graphite. For instance, the densities of $ZnCo_2O_4$ and graphite are 5.46 and 2.25 g/cm^3, respectively. Higher densities are beneficial to higher energy densities. Lastly, the negative potential of metal oxides are higher than that of graphite, which can prevent the formation of lithium dendrites and help enhance security [7, 8]. Zinc cobaltate (ZCO), for example, presents a high theoretical specific capacity (900 mA h/g), which is 2–3 times compared with that of graphite electrodes [9]. However, ZCO electrodes have poor electronic conductivity and low Li^+ diffusivity. Moreover, the structural stability during the charging/discharging process is also unsatisfying because of the large volume change upon charge/discharge. These factors lead to the poor rate performance and rapid capacity fading, thus hindering the widespread application of ZCO electrodes.

To meet the above challenges, several material design strategies have been developed in recent years. To reduce the pathway length for Li^+ diffusion in the electrode materials, various ZCO nanostructures have been constructed [10, 11, 12, 13, 14, 15, 16, 17, 18]. The strategy of using nanocarbons such as graphene, carbon nanotubes, and mesoporous carbon [19,

https://doi.org/10.1557/jmr.2019.258 Published online by Cambridge University Press

© Materials Research Society 2019

20, 21] as conductive matrices to grow ZCO nanostructures is further developed. On one hand, it can reduce the ZCO particle size. On the other hand, it can facilitate the electron conduction capability, thus improving the lithium storage kinetics. Despite the significant advances that have been achieved, the low packing densities of nano-sized materials inevitably decrease the volumetric energy storage capacity of the whole cell. Besides, those carbon additives also result in lowering the specific capacity of electrode materials, making ZCO deviate from the way to practical application. Therefore, improving the lithium storage kinetics and stability within a compact ZCO electrode is impressing but still quite challenging.

In recent years, ion doping has been considered as an effective method to modify the inherent physicochemical properties of metal compounds [22]. The doping element may induce charge redistribution, which provides an opportunity to improve the electronic/ionic conductivity of electrode materials. Particularly, the doped metal oxide electrodes of LIBs can accelerate the electronic and ionic transport, thereby contributing to better electrochemical performance. For example, Bi-doped lithium titanium oxides were prepared by Lee et al. [23] It reduces the electrode polarization and enhances the conductivity, which endows the resultant $Li_4Ti_{4.9}Bi_{0.10}O_{12}$ electrode with higher reversible capacity, more stable cycling performance, and the enhanced rate capability compared with the undoped electrodes. Xu et al. synthesized the P-doped WO_{3-x} with P dopant greatly promoting the lithium storage kinetics [24]. Wang et al. synthesized ultra-thin black TiO_{2-x} nanoflakes with rich oxygen vacancies, which demonstrates the electrochemical performance improvement in rechargeable Mg batteries [25].

Inspired by the above research achievements, here we designed and fabricated nitrogen-doped zinc/cobalt mixed oxide (N-ZCO) micro-/nanospheres through a facile NH_4HCO_3-assisted calcination process. As-prepared N-ZCO shows a compact electrode structure. We improved the enhancement of nitrogen doping in lithium storage. Nitrogen doping on one hand improves the electronic conduction capability and Li^+ diffusivity, and on the other hand, it enhances the structural stability of the electrode. As a result, N-ZCO demonstrates excellent rate capability and long-term cyclability. At the current density of 5 A/g, it delivers a high capacity retention rate of 65% based on the initial capacity. Moreover, the N-ZCO electrode shows as high as 978 mA h/g after 500 cycles at the current density of 1 A/g. These outstanding lithium storage properties make the N-ZCO electrodes a promising anode candidate in the next-generation LIBs. Furthermore, our work suggests that the introduction of nitrogen into transition metal oxide electrode materials could be an effective approach to improve the electrode performance for rechargeable LIBs.

Results and discussion

The scanning electron microscopy (SEM) images shown in Figs. 1(a)–1(d) display the morphology of ZCO spheres and as-obtained N-ZCO spheres. The ZCO spheres are very uniform and the diameters range from 1 to 2 μm [Fig. 1(a)]. From Fig. 1(b), we can see that each ZCO microsphere comprised numerous nanoparticle subunits with the size of several tens of nanometres. After high-temperature annealing with the nitrogen source, the spherical morphology was well maintained. The particle size of as-obtained N-ZCO microspheres slightly increases with the diameter in the range of 2–3 μm [Fig. 1(c)]. Moreover, it can be seen from Fig. 1(d) that the subunit particle size increases to several hundreds of nanometres, which is almost an order of magnitude higher than that of ZCO. Such observation results indicate that the crystal regrowth process occurs during the annealing process. The main chemical compositions and element distribution of N-ZCO are evidenced by energy-dispersive X-ray spectroscopy (EDS). From Fig. 1(e), we can see that the Zn, Co, O, and N elements are uniformly distributed throughout the whole N-ZCO spheres, indicating the introduction of N dopant.

The crystallinity structures and composition phases of two samples were checked by the X-ray diffraction (XRD) technique. As shown in Fig. 2(a), all the peaks of ZCO spheres are indexed to the standard $ZnCo_2O_4$ phase (JCPDS No. 23-1390, space group $Fd\bar{3}m$, $a = b = c = 8.44$ Å), and no other impurities were detected, indicating its high purity. After N

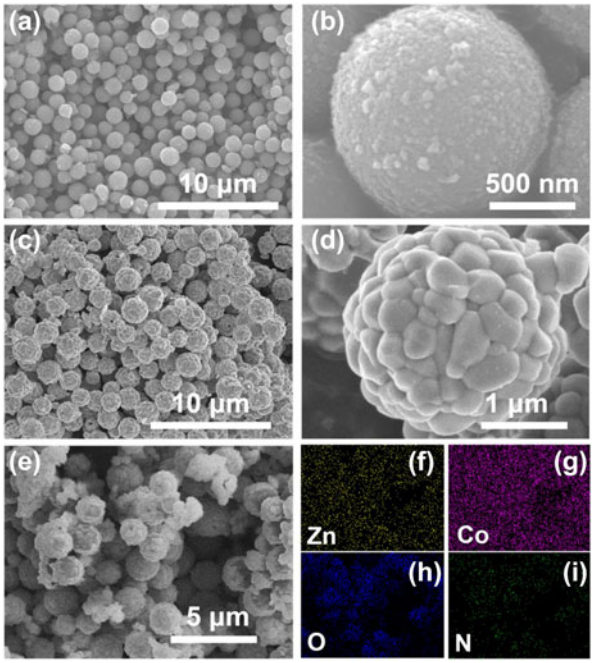


Figure 1: SEM images of ZCO spheres (a, b) and N-ZCO spheres (c, d). (e–i) EDS mapping of N-ZCO: (e) SEM image of N-ZCO, corresponding elemental mapping of (f) Zn, (g) Co, (h) O, (i) N.

https://doi.org/10.1557/jmr.2019.258 Published online by Cambridge University Press

© Materials Research Society 2019

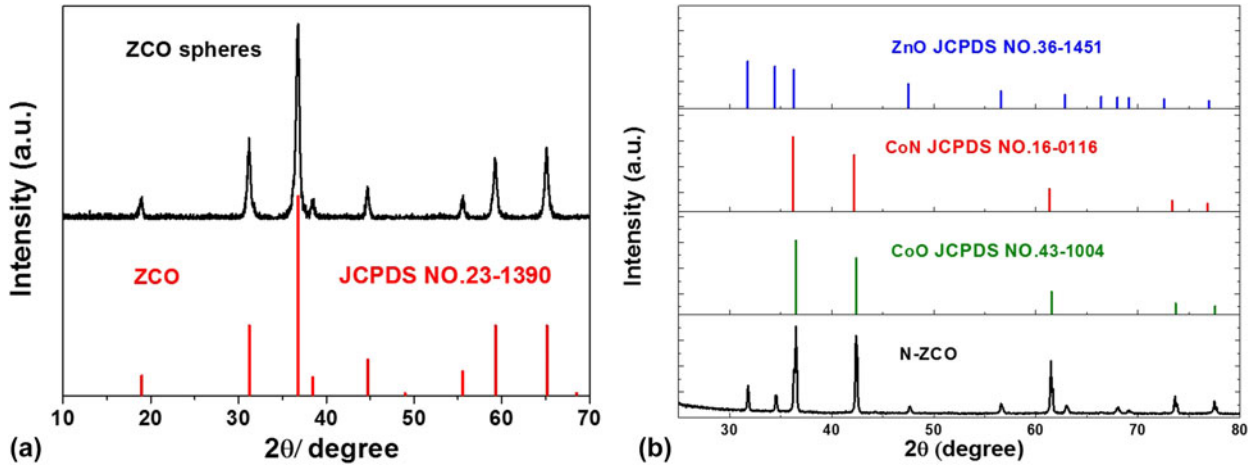


Figure 2: XRD patterns of the as-prepared (a) ZCO and (b) N-doped ZnO/CoO.

doping, as shown in Fig. 2(b), the ZCO phase transformed to a mixture of CoO (JCPDS No. 43-1004, space group $Fm3m$, $a = b = c = 4.26$ Å), CoN (JCPDS No. 16-0116, space group $F\bar{4}3m$, $a = b = c = 4.28$ Å), and ZnO (JCPDS No. 36-1451, space group $P6_3mc$, $a = b = 3.25$ Å, $c = 5.21$ Å), confirming the successful doping of nitrogen in the ZCO sample.

To further explore the elemental composition and chemical states of two samples, X-ray photoelectron spectroscopy (XPS) was applied to check the as-prepared ZCO and N-ZCO. Figure 3(a) displays the wide spectrum of two samples, and the high-resolution spectra of Zn, Co, O, N, and C elements are shown in Figs. 3(b)–3(f), respectively. As shown in Fig. 3(b), the peaks at 1021 and 1044.1 eV are assigned to Zn $2p_{3/2}$ and Zn $2p_{1/2}$, respectively [26]. It is worth noting that the corresponding peaks of Zn $2p$ for N-ZCO sample shift to higher binding energies of 1021.7 and 1044.8 eV, respectively. This should be ascribed to the introduction of N dopant, which leads to the changes in charge distribution [27, 28]. A similar phenomenon also happened among Co and O elements [Figs. 3(c) and 3(d)]. The XPS peak fitting shows that N 1s spectrum is made up of metal nitrides (397.5 eV) and pyrrolic N (399.3 eV), which further confirms the successful doping of the N element. The C 1s spectrum could be divided into two peaks, including carbide C (282.9 eV) and C–O (286.8 eV). The doping of nitrogen in ZCO can alter the distribution of the electron and increase the conductivity.

CR2032 coin cells were used to evaluate the electrochemical performance of two electrodes. Figures 4(a) and 4(b) display the cyclic voltammetry (CV) curves of ZCO and N-ZCO electrodes during the first, second, third, and fourth cycles at a scan rate of 0.2 mV/s. As we can see from Fig. 4(a), the sharp and large reduction peak at ~0.78 V in the first cathodic scan is related to the destruction of the ZCO crystal structure and the formation of metallic Zn and Co nanoparticles, as well as the formation of a solid electrolyte interphase (SEI) [10]. In the first anodic scan, the peaks around 1.7 V and 2.2 V are due to the oxidation of Zn to ZnO and Co to Co_3O_4, respectively. From the second scan, the reduction peaks move to a higher position of ~1 V, indicating the irreversible electrochemical reaction in the first lithiation process. Noticeably, the CV curves of the N-ZCO electrode in Fig. 4(b) are quite different from that of the ZCO electrode in Fig. 4(a). In the first cathodic scan, a strong peak is observed at ~0.3 V, followed by a low intensity peak at ~0.2 V; these two peaks are attributed to a combination of several electrochemical reactions at close potentials, such as the lithiation process of ZnO and CoN to form Zn, Co, Li_2O, and Li_3N, the alloying reaction between Zn and Li, and the formation of a gel-like SEI layer [29]. In the first anodic scan, the peaks around 0.7, 1.7, and 2 V should be ascribed to the multistep delithiation process of Li_3N [30, 31]. Meanwhile, the peak located at ~0.7 V is also associated with the dealloying reaction of Li–Zn alloy, and the weak peak at ~1.4 V corresponds to convention of Zn to ZnO. From the second sweep, both cathodic and anodic peaks display a positive shift in potentials. Besides, the CV curves overlap well from the second scan, indicating the good reversibility. The discharge/charge profiles of ZCO and N-ZCO during the first, second, 10th, and 50th cycles at a current density of 0.2 A/g are shown in Figs. 4(c) and 4(d). Similar to the CV curves in Figs. 4(a) and 4(b), the first discharge/charge curves of the two samples are quite different from the second ones, implying the unique lithium storage mechanism in the first cycle. During the first discharge cycle in Fig. 4(c), the voltage drops sharply from the open-circuit voltage (OCV) to about 1 V. This is owing to the beginning of the insertion of Li^+ ions into the ZCO structure. The long voltage plateau at around 1 V in the ZCO electrode during the first discharge process is related to the reaction from ZCO to Zn and Co [Fig. 4(c)]. As to the N-ZCO electrode [Fig. 4(d)], the corresponding plateau moves to a much lower value of about 0.5 V, which suggests that the introduction of the N

https://doi.org/10.1557/jmr.2019.258 Published online by Cambridge University Press

© Materials Research Society 2019

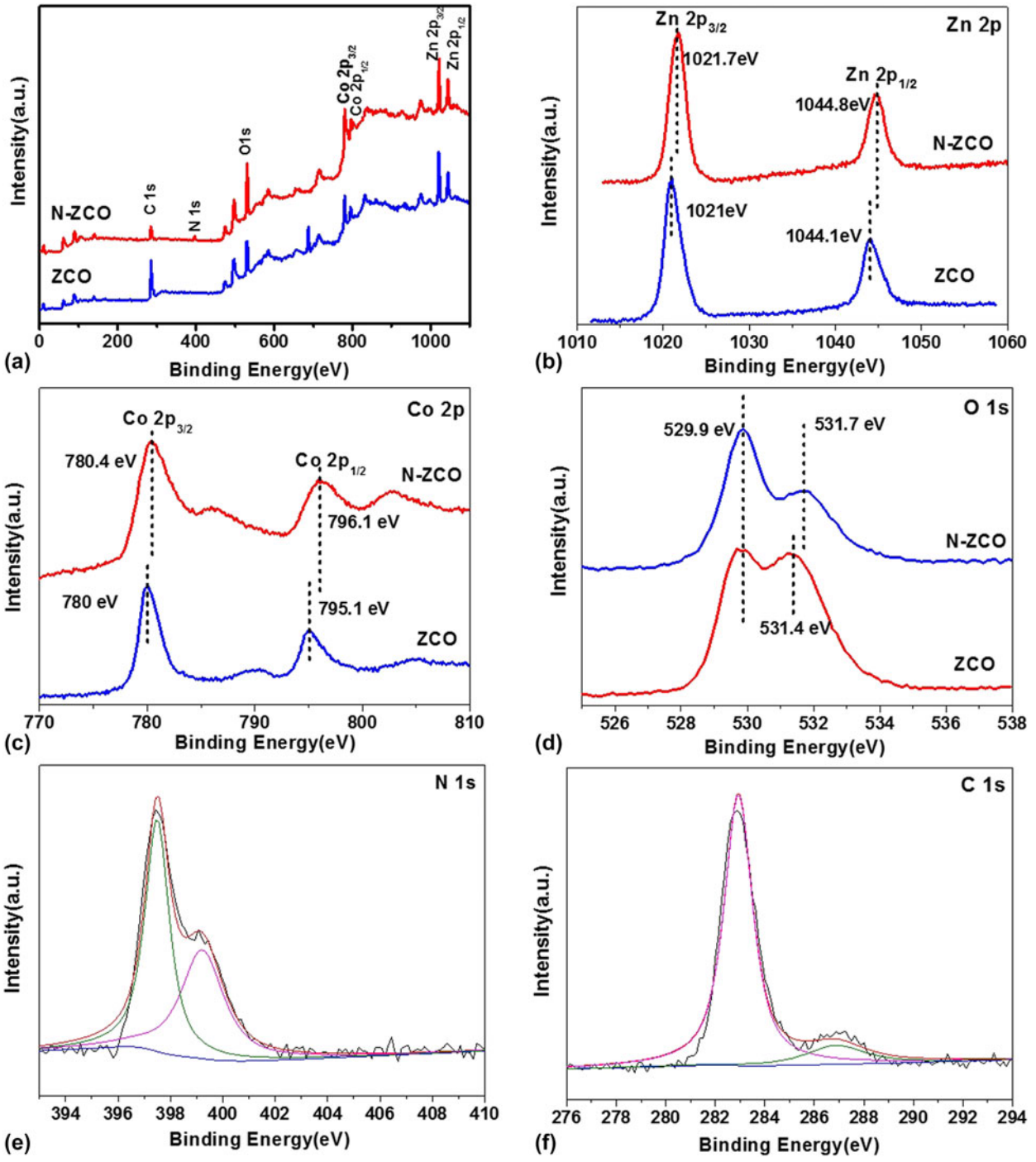


Figure 3: (a) XPS survey scan spectrum of ZCO and N-ZCO. High-resolution XPS spectrum of Zn 2*p* (b), Co 2*p* (c), O 1*s* (d), N 1*s* (e), and C 1*s* (f).

element can reduce the lithium storage voltage of the electrode material. Moreover, the first discharge and charge capacity of the ZCO electrode are 1282.4 and 911.3 mA h/g, respectively, corresponding to a Coulombic efficiency of ~71%. The initial discharge and charge capacity of the N-ZCO electrode are 1303.9 and 936.9 mA h/g, respectively. The initial Coulombic efficiency of the N-ZCO electrode is ~72%, similar to that of the ZCO electrode. The irreversible capacity loss of the two electrodes mainly originate from the irreversible consumption of lithium ions during the first charging/discharging process, which includes the incomplete decomposition of Li_2O and Li_3N, as well as the formation of the SEI layer [32, 33].

The rate capability of electrode materials is particularly important when batteries are used as the energy carrier of electric vehicles. Here, the as-obtained two electrodes were

https://doi.org/10.1557/jmr.2019.258 Published online by Cambridge University Press

© Materials Research Society 2019

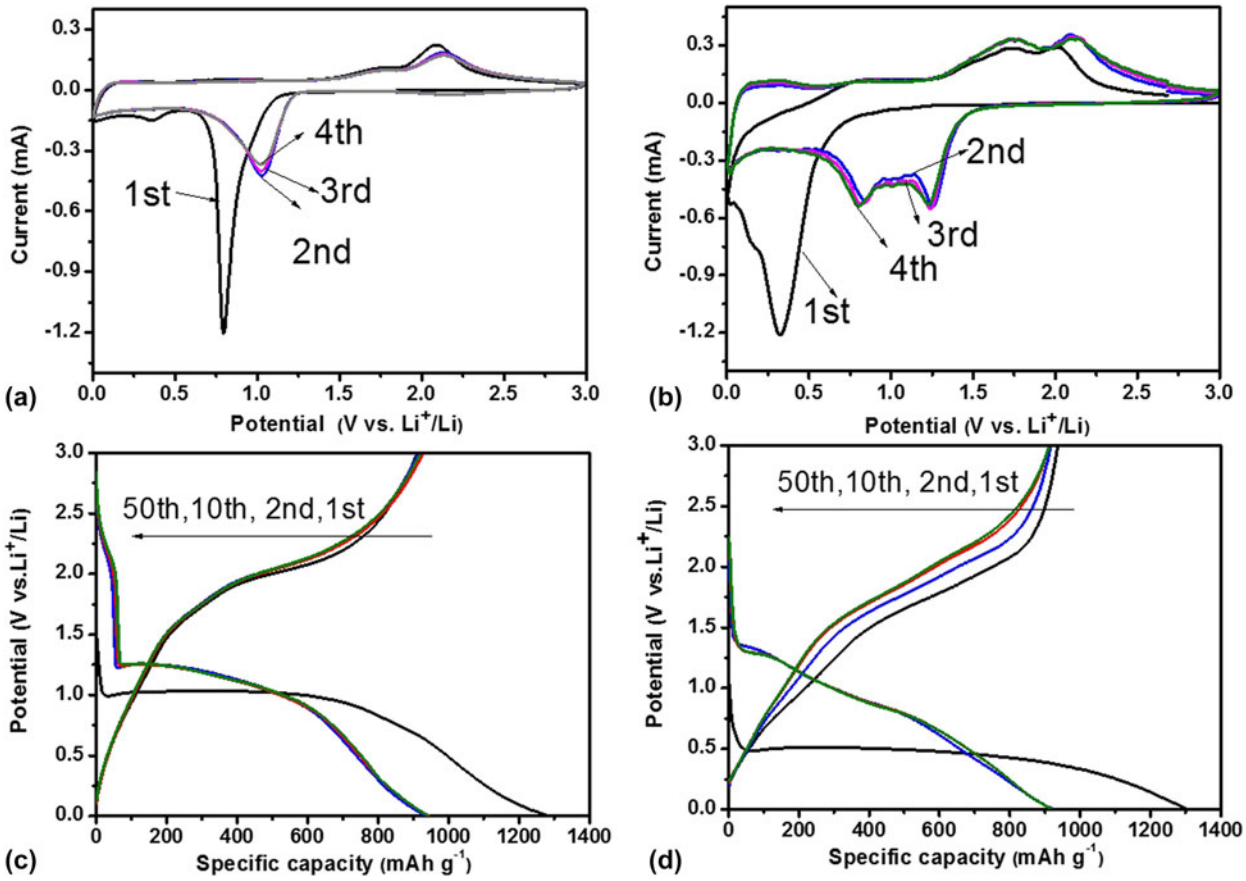


Figure 4: CV curves of ZCO (a) and N-ZCO (b) electrodes with a scan rate of 0.2 mV/s. The galvanostatic discharge/charge curves of ZCO (c) and N-ZCO (d) electrodes at a current density of 0.2 A/g.

tested at different current densities from 0.2 to 5 A/g to explore the rate capability. As can be seen from Fig. 5(a), a high reversible capacity of 924 mA h/g is achieved for the N-ZCO electrode at a current density of 0.2 A/g with a Coulombic efficiency of 72.8%. When the current density was raised to 0.5, 1, and 2 A/g, the N-ZCO electrode still delivered reversible capacities of 917, 876, and 736 mA h/g, respectively. Even at a high rate of 5 A/g, it can still present a high capacity of 605 mA h/g, corresponding to a 65% capacity retention rate based on the initial capacity at 0.2 A/g. When the current density was returned to 0.2 A/g, the specific capacity could recover back at 977 mA h/g, even higher than the initial reversible capacity. This phenomenon is due to a gradual activated process, which is caused by the reversible formation/dissolution of a gel-like polymer layer on the surface of the active material [34]. In contrast, the ZCO electrodes show relatively poor rate capability. At a high current density of 5 A/g, the ZCO electrode can only deliver a reversible capacity of 335 mA h/g, and the capacity retention rate is only 36.7%, much lower than that of the N-ZCO electrode, implying the boosted lithium storage kinetics and excellent electrochemical reversibility of the N-ZCO electrode. We then tested the cycling performance of the two samples. The cycling performance of the N-ZCO electrode was measured at a current density of 0.2 A/g as shown in Fig. 5(b). It can be seen that the first discharge and charge capacities of the N-ZCO electrode are 1251 and 912 mA h/g, respectively, corresponding to a Coulombic efficiency of 72.9%. It delivered a high reversible capacity of 1055 mA h/g after 100 cycles, again demonstrating the good cycling stability. The cycling comparison of ZCO and N-ZCO electrodes at a current density of 1 A/g are presented in Fig. 5(c). The specific capacity of the N-ZCO electrode decreased a little during the initial 20 cycles, after that, it showed an upward trend, and a high capacity of 978 mA h/g remained after 500 cycles. Such capacity activation process has also been reported before, which is ascribed to the reversible formation and decomposition of the gel-like polymer film [35, 36]. By contrast, the ZCO electrode shows obvious capacity decay over prolonged cycling, with only a low capacity of 260 mA h/g received after 500 cycles. Such result suggests the much improved cycling performance and structural stability of the N-ZCO electrode compared with the ZCO electrode.

Electrochemical impedance spectroscopy (EIS) was further conducted to reveal the kinetic processes of two electrodes, and

https://doi.org/10.1557/jmr.2019.258 Published online by Cambridge University Press

© Materials Research Society 2019

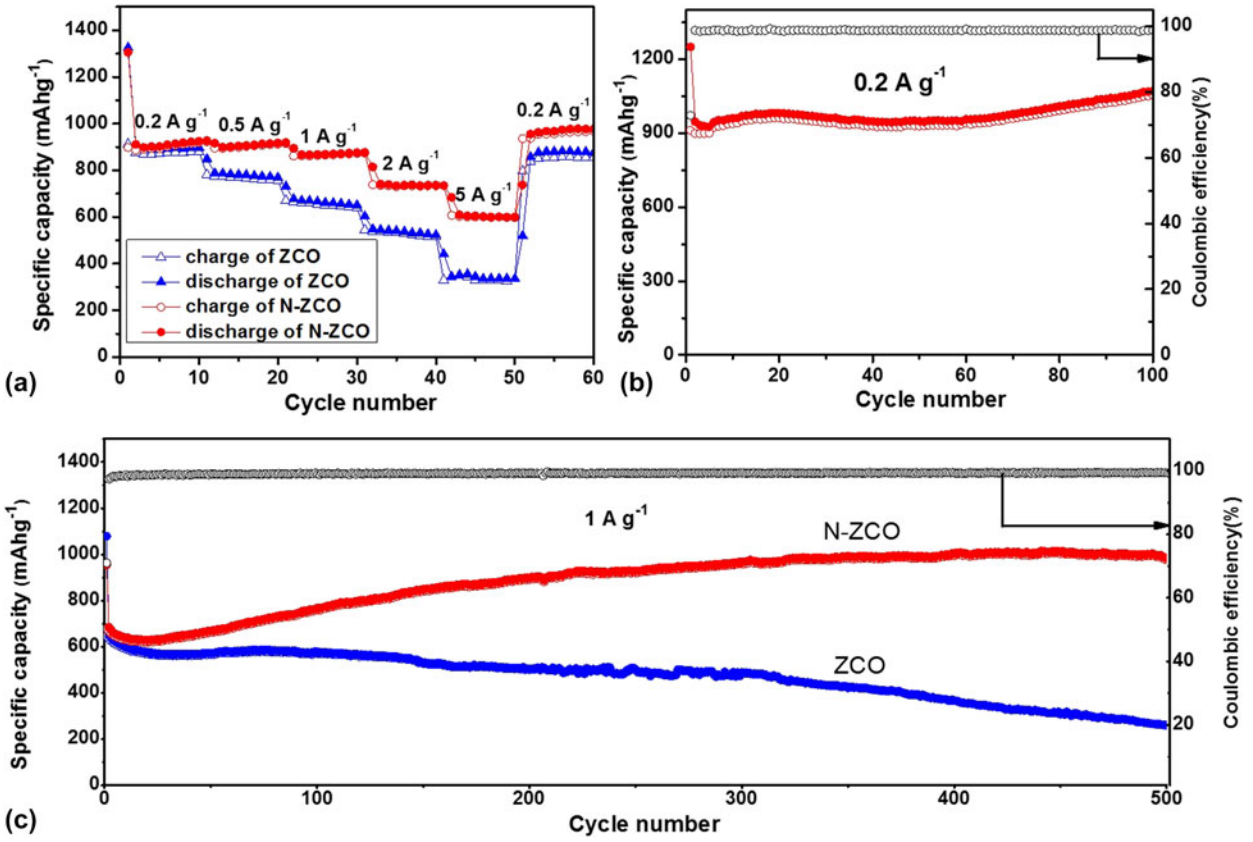


Figure 5: (a) Rate performance of ZCO and N-ZCO electrodes at different current densities ranging from 0.2 to 5 A/g. (b) Cycling performance of the N-ZCO electrode at a current density of 0.2 A/g. (c) Cycling performance of ZCO and N-ZCO electrodes at a current density of 1 A/g.

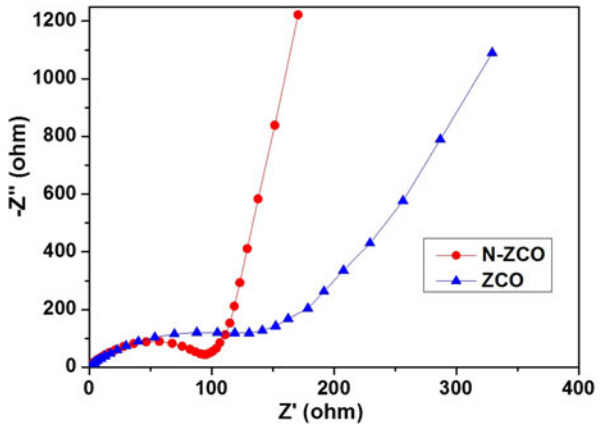


Figure 6: Impedance analysis of the ZCO and N-ZCO electrodes in their original states.

Fig. 6 shows the resulting Nyquist curves. The intercept on the X axis represents the electron conduction resistance (R_e). The semicircle in the high-middle frequency range corresponds to the charge-transfer process, and the sloping line in the low-frequency range is related to the lithium-ion diffusion process [37]. The R_e value of N-ZCO is lower than ZCO (1.3 versus 2.7 ohm), indicating the improved electron conducting capability after nitrogen doping. The enhanced electronic conductivity has also been confirmed by a four-probe conductivity. N-ZCO shows a much higher electronic conductivity (2.3×10^{-5} S/cm) than ZCO (5.6×10^{-6} S cm^{-1}). The smaller semicircle diameter of N-ZCO compared with ZCO suggests a faster charge transfer process. Moreover, the larger slope line in the low-frequency range implies much higher Li^+ diffusivity of the N-ZCO electrode than that of the ZCO electrode. These three factors result in much faster lithium storage kinetics in the N-ZCO electrode than the ZCO electrode.

Conclusion

In summary, we have developed a facile N-doped strategy to modify the electronic properties of ZCO and demonstrated its potential as high-performance anodes in LIBs. Electrochemical studies proved that the nitrogen dopant can improve electronic conductivity and accelerate the lithium-ion diffusion, potentially endowing the N-ZCO electrode with much improved high-rate capability and cycling stability compared with ZCO. The atomic substitution strategy is simple and can be extended to other transition metal oxides. Our findings will provide new opportunities for developing electrode materials of LIBs with high-rate capability and long-term cycling stability.

https://doi.org/10.1557/jmr.2019.258 Published online by Cambridge University Press

© Materials Research Society 2019

Experimental

Preparation of $ZnCo_2O_4$ micro-/nanospheres

In a typical synthesis, polyvinylpyrrolidone (PVP, MW ~ 580,000, 0.1 g) was dispersed in 50 mL of ethylene glycol (EG) under vigorous stirring for about half an hour to form a transparent solution. After that, $Zn(Ac)_2{\cdot}2H_2O$ (1 mmol) and $Co(Ac)_2{\cdot}4H_2O$ (2 mmol) were added to the solution with continuous stirring. Then, the above homogeneous solution was transferred to a 100-mL Teflon-lined stainless steel autoclave, which was placed in an oven. The temperature was gradually increased to 200 °C within an hour and subsequently maintained at 200 °C for another 24 h. After naturally cooling down to room temperature, the resultant precipitate was centrifuged and washed with deionized water and ethyl alcohol for several times and then dried in an oven at 80 °C for 12 h. Finally, the products are thermally decomposed in a muffle oven under air atmosphere, which was maintained at 500 °C for 3 h with a heating rate of 2 °C/min, forming the ZCO micro-/nanospheres.

Preparation of N-doped ZCO/CoO micro-/nanospheres

Typically, ZCO micro-/nanospheres (0.1 g) and NH_4HCO_3 (6 g) were mixed by grinding with an agate mortar for an hour. Then, the mixture were placed in a porcelain boat and annealed in a tube furnace under Ar atmosphere at 800 °C for 2 h, with a heating rate of 5 °C/min, forming the N-doped ZCO/CoO micro-/nanospheres, named N-ZCO.

Materials characterization

The phase composition and crystalline structure of the products were characterized by X-ray diffraction (XRD) using a Bruker D8, Bruker, Germany, equipped with a Cu K_α radiation source (λ = 1.54178 Å). The morphology and the elements dispersion of the two samples were observed by scanning electron microscopy (SEM; JEOL, JSM-7001F, Japan). X-ray photoelectron spectroscopy (XPS) of as-prepared ZCO and N-doped ZnO/CoO were measured on a PerkinElmer model PHI 5600 XPS system, PerkinElmer, with an Al K_α X-ray source.

Electrochemical measurements

The electrochemical performance of two samples was tested by using the CR2032 coin cell. The electrodes were prepared by mixing the active materials, acetylene black and polyvinylidene fluoride (PVDF), in *N*-methyl-2-pyrrolidinone (NMP, Sigma-Aldrich, Shanghai, China) at a weight ratio of 8:1:1. The mixture was stirred for 6 h and then was coated onto a copper foil and dried in an oven at 80 °C for 24 h. The electrode pieces were processed into small round pieces with a diameter of 12 mm by a chipper. The mass loading of each electrode was about 1 mg/cm^2. The coin cells were assembled in an Ar-filled glovebox using Celgard 2400 as the separator, lithium foil as the reference electrode, and 1 mol/L $LiPF_6$ in EC:DEC = 1:1 (v/v) as the electrolyte. The CV curves and EIS were recorded on a VMP3 electrochemical station, the scan rate of CV test was 0.2 mV/s, the voltage range is set from 0.01 to 3 V, and the testing frequency range for EIS was set from 100 kHz to 10 mHz. The galvanostatic charge/discharge curves were tested on a Land CT2001A (BRTBTS, Wuhan, China) multichannel battery test system between 0.01 and 3 V. The specific capacity was calculated based on the mass loading of the active material.

Acknowledgments

The authors acknowledge the financial support of the National Natural Science Foundation of China (51502147), Natural Science Foundation of Inner Mongolia (2015BS0510), China Postdoctoral Science Foundation (2017M611205), Fund of Key Laboratory of Advanced Materials of Ministry of Education (No. 2016AML08), Inner Mongolia scientific and technological achievements transformation project (CGZH2018132), and Inner Mongolia Innovation project for postgraduates (Nos. B20171012804Z and S20171012807).

References

1. **A. Manthiram**: Materials challenges and opportunities of lithium ion batteries. *J. Phys. Chem. Lett.* **2**, 373 (2011).
2. **L. Lu, X. Han, J. Li, J. Hua, and M. Ouyang**: A review on the key issues for lithium-ion battery management in electric vehicles. *J. Power Sources* **226**, 272 (2013).
3. **B. Scrosati, J. Hassoun, and Y-K. Sun**: Lithium-ion batteries. A look into the future. *Energy Environ. Sci.* **4**, 3287 (2011).
4. **L. Shen, S. Chen, J. Maier, and Y. Yu**: Carbon-coated Li_3VO_4 spheres as constituents of an advanced anode material for high-rate long-life lithium-ion batteries. *Adv. Mater.* **29**, 1701571–1701577 (2017).
5. **X. Xu, R. Zhao, W. Ai, B. Chen, H. Du, L. Wu, H. Zhang, W. Huang, and T. Yu**: Controllable design of MoS_2 nanosheets anchored on nitrogen-doped graphene: Toward fast sodium storage by tunable pseudocapacitance. *Adv. Mater.* **30**, 1800658–1800664 (2018).
6. **M.R. Lukatskaya, B. Dunn, and Y. Gogotsi**: Multidimensional materials and device architectures for future hybrid energy storage. *Nat. Commun.* **7**, 12647–12659 (2016).
7. **P. Poizot, S. Laruelle, S. Grugeon, L. Dupont, and J.M. Tarascon**: Nano-sized transition-metal oxides as negative-electrode materials for lithium-ion batteries. *Nature* **407**, 496 (2000).
8. **L. Ji, Z. Lin, M. Alcoutlabi, and X. Zhang**: Recent developments in nanostructured anode materials for rechargeable lithium-ion batteries. *Energy Environ. Sci.* **4**, 2682 (2011).

https://doi.org/10.1557/jmr.2019.258 Published online by Cambridge University Press

© Materials Research Society 2019

9. **D. Jiaojiao, Y. Xiaoliang, H. Yanbing, L. Baohua, Y. Quan-Hong, and K. Feiyu**: A sliced orange-shaped $ZnCo_2O_4$ material as anode for high-performance lithium ion battery. *Energy Storage Mater.* **6**, 61 (2017).
10. **Y. Sharma, N. Sharma, G.V.S. Rao, and B.V.R. Chowdari**: Nanophase $ZnCo_2O_4$ as a high performance anode material for Li-ion batteries. *Adv. Funct. Mater.* **17**, 2855 (2007).
11. **N. Du, Y. Xu, H. Zhang, J. Yu, C. Zhai, and D. Yang**: Porous $ZnCo_2O_4$ nanowires synthesis via sacrificial templates: High-performance anode materials of Li-ion batteries. *Inorg. Chem.* **50**, 3320 (2011).
12. **H. Liu and J. Wang**: One-pot synthesis of $ZnCo_2O_4$ nanorod anodes for high power lithium ions batteries. *Electrochim. Acta* **92**, 371 (2013).
13. **W. Luo, X. Hu, Y. Sun, and Y. Huang**: Electrospun porous $ZnCo_2O_4$ nanotubes as a high-performance anode material for lithium-ion batteries. *J. Mater. Chem.* **22**, 8916 (2012).
14. **Z. Wang, L. Zhou, and X.W. Lou**: Metal oxide hollow nanostructures for lithium-ion batteries. *Adv. Mater.* **24**, 1903 (2012).
15. **Y. Zhu, C. Cao, J. Zhang, and X. Xu**: Two-dimensional ultrathin $ZnCo_2O_4$ nanosheets: General formation and lithium storage application. *J. Mater. Chem. A* **3**, 9556 (2015).
16. **Y. Zhao, X. Li, B. Yan, D. Xiong, D. Li, S. Lawes, and X. Sun**: Recent developments and understanding of novel mixed transition-metal oxides as anodes in lithium ion batteries. *Adv. Energy Mater.* **6**, 1502175 (2016).
17. **J. Mei, T. Liao, L. Kou, and Z. Sun**: Two-Dimensional metal oxide nanomaterials for next-generation rechargeable batteries. *Adv. Mater.* **29**, 1700176 (2017).
18. **J. Mei, T. Liao, H. Spratt, G.A. Ayoko, X. Zhao, and Z. Sun**: Honeycomb-inspired heterogeneous bimetallic Co–Mo oxide nanoarchitectures for high-rate electrochemical lithium storage. *Small Methods* **3**, 1900055 (2019).
19. **A.K. Rai, T. Trang Vu, B.J. Paul, and J. Kim**: Synthesis of nano-sized $ZnCo_2O_4$ anchored with graphene nanosheets as an anode material for secondary lithium ion batteries. *Electrochim. Acta* **146**, 577 (2014).
20. **B. Liu, X. Wang, B. Liu, Q. Wang, D. Tan, W. Song, X. Hou, D. Chen, and G. Shen**: Advanced rechargeable lithium-ion batteries based on bendable $ZnCo_2O_4$-urchins-on-carbon-fibers electrodes. *Nano Res.* **6**, 525 (2013).
21. **Q. Ru, X. Song, Y. Mo, L. Guo, and S. Hu**: Carbon nanotubes modified for $ZnCo_2O_4$ with a novel porous polyhedral structure as anodes for lithium ion batteries with improved performances. *J. Alloys Compd.* **654**, 586 (2016).
22. **Y. Chunshuang, Z. Yue, L. Yutao, F. Zhiwei, P. Lele, Z. Xin, C. Gang, and Y. Guihua**: Local built-in electric field enabled in carbon-doped Co_3O_4 nanocrystals for superior lithium-ion storage. *Adv. Funct. Mater.* **28**, 1705951 (2018).
23. **T. Subburaj, K. Prasanna, K.J. Kim, P.R. Ilango, Y.N. Jo, and C.W. Lee**: Structural and electrochemical evaluation of bismuth doped lithium titanium oxides for lithium ion batteries. *J. Power Sources* **280**, 23 (2015).
24. **J. Xu, Z. Liao, J. Zhang, B. Gao, P.K. Chu, and K. Huo**: Heterogeneous phosphorus-doped WO_{3-x}/nitrogen-doped carbon nanowires with high rate and long life for advanced lithium-ion capacitors. *J. Mater. Chem. A* **6**, 6916 (2018).
25. **Y. Wang, X. Xue, P. Liu, C. Wang, X. Yi, Y. Hu, L. Ma, G. Zhu, R. Chen, and T. Chen**: Atomic substitution enabled synthesis of vacancy-rich two-dimensional black TiO_{2-x} nanoflakes for high-performance rechargeable magnesium batteries. *ACS Nano* **12**, 12492 (2018).
26. **G. Wu, Z. Jia, Y. Cheng, H. Zhang, X. Zhou, and H. Wu**: Easy synthesis of multi-shelled ZnO hollow spheres and their conversion into hedgehog-like ZnO hollow spheres with superior rate performance for lithium ion batteries. *Appl. Surf. Sci.* **464**, 472 (2019).
27. **M. Xu, S. He, H. Chen, G. Cui, L. Zheng, B. Wang, and M. Wei**: TiO_{2-x}-modified ni nanocatalyst with tunable metal–support interaction for water–gas shift reaction. *ACS Catal.* **7**, 7600 (2017).
28. **S. Liu, J. Zhou, and H. Song**: 2D Zn-hexamine coordination frameworks and their derived N-rich porous carbon nanosheets for ultrafast sodium storage. *Adv. Energy Mater.* **8**, 1800569 (2018).
29. **X. Huang, X. Xia, Y. Yuan, and F. Zhou**: Porous ZnO nanosheets grown on copper substrates as anodes for lithium ion batteries. *Electrochim. Acta* **56**, 4960 (2011).
30. **B. Das, M. Reddy, G.S. Rao, and B. Chowdari**: Synthesis of porous-CoN nanoparticles and their application as a high capacity anode for lithium-ion batteries. *J. Mater. Chem.* **22**, 17505 (2012).
31. **B. Das, M. Reddy, P. Malar, T. Osipowicz, G.S. Rao, and B. Chowdari**: Nanoflake CoN as a high capacity anode for Li-ion batteries. *Solid State Ionics* **180**, 1061 (2009).
32. **J. Deng, X. Yu, X. Qin, B. Li, and F. Kang**: Carbon sphere-templated synthesis of porous yolk–shell $ZnCo_2O_4$ spheres for high-performance lithium storage. *J. Alloys Compd.* **780**, 65 (2019).
33. **J. Deng, X. Yu, X. Qin, D. Zhou, L. Zhang, H. Duan, F. Kang, B. Li, and G. Wang**: Co–B nanoflakes as multifunctional bridges in $ZnCo_2O_4$ micro-/nanospheres for superior lithium storage with boosted kinetics and stability. *Adv. Energy Mater.* **9**, 1803612 (2019).
34. **J. Deng, X. Yu, X. Qin, B. Liu, Y-B. He, B. Li, and F. Kang**: Controlled synthesis of anisotropic hollow $ZnCo_2O_4$ octahedrons for high-performance lithium storage. *Energy Storage Mater.* **11**, 184 (2018).
35. **J. Deng, X. Yu, Y. He, B. Li, Q-H. Yang, and F. Kang**: A sliced orange-shaped $ZnCo_2O_4$ material as anode for high-performance lithium ion battery. *Energy Storage Mater.* **6**, 61 (2017).
36. **Y. Jiang, Y. Song, Z. Pan, Y. Meng, L. Jiang, Z. Wu, P. Yang, Q. Gu, D. Sun, and L. Hu**: Rapid amorphization in metastable $CoSeO_3 \cdot H_2O$ nanosheets for ultrafast lithiation kinetics. *ACS Nano* **12**, 5011 (2018).
37. **Y. Li, Y. Zhao, C. Ma, and Y. Zhao**: Promising carbon matrix derived from willow catkins for the synthesis of SnO_2/C composites with enhanced electrical performance for Li-ion batteries. *Nano* **13**, 1850087 (2018).

https://doi.org/10.1557/jmr.2019.258 Published online by Cambridge University Press

© Materials Research Society 2019